DESY Report

arXiv:1012.6037v1 [hep-ph] 29 Dec 2010

Forward-Central Jet Correlations at the Large Hadron Collider

M. Deak[a], F. Hautmann[b], H. Jung[c,d] and K. Kutak[d]

[a]Instituto de Física Teórica UAM/CSIC, Facultad de Ciencias, C-XI,
Universidad Autónoma de Madrid, Cantoblanco, Madrid 28049

[b]Theoretical Physics Department, University of Oxford, Oxford OX1 3NP

[c]Deutsches Elektronen Synchrotron, D-22603 Hamburg

[d] Elementaire Deeltjes Fysica, Universiteit Antwerpen, B 2020 Antwerpen

Abstract

For high-p_T forward processes at the Large Hadron Collider (LHC), QCD logarithmic corrections in the hard transverse momentum and in the large rapidity interval may both be quantitatively significant. The theoretical framework to resum consistently both kinds of logarithmic corrections to higher orders in perturbation theory is based on QCD high-energy factorization. We present numerical Monte Carlo applications of this method to final-state observables associated with production of one forward and one central jet. By computing jet correlations in rapidity and azimuth, we analyze the role of corrections to the parton-showering chain from large-angle gluon radiation, and discuss this in relationship with Monte Carlo results modeling interactions due to multiple parton chains.

1 Introduction

Physics in the forward region at hadron colliders is traditionally dominated by soft particle production. With the advent of the LHC, forward physics phenomenology turns into a largely new field [1–3] involving both soft and hard production processes, because of the phase space opening up at high center-of-mass energies. Owing to the unprecedented reach in rapidity of the experimental instrumentation, it becomes possible to carry out a program of high-p_T physics in the forward region.

Forward jet production enters the LHC physics program in an essential way both for QCD studies and for new particle searches, e.g. in vector boson fusion search channels for the Higgs boson [4, 5]. Another area of potential interest in forward physics employs near-beam proton taggers [6]: this will enable studies to be made in the central high-p_T production mode with forward protons, which can be used for both standard-candle [7]

and discovery physics [8]. In addition to collider physics applications, measurements of forward particle production at the LHC will serve as input to the modeling of high-energy air showers in cosmic ray experiments [9].

The forward production of high-p_T particles brings jet physics into a region characterized by multiple energy scales and asymmetric parton kinematics. In this multi-scale region it is compelling to ask [2, 10] whether fixed-order next-to-leading calculations reliably describe the production process or significant contributions arise beyond fixed order which call for perturbative QCD resummations. The early observation [11] of potentially large logarithmic corrections to jet production at asymptotically high energies has given rise to an ample literature of calculations based on the BFKL equation [12–15]. On the other hand, at collider energies both logarithmic corrections in the large rapidity interval (of high-energy type) and logarithmic corrections in the hard transverse momentum (of collinear type) are phenomenologically important. The theoretical framework to resum consistently both kinds of logarithmic corrections in QCD perturbation theory is based on high-energy factorization at fixed transverse momentum [16]. This factorization program is carried through in [17] for forward jet hadroproduction.

In this paper we present the application of the results [17] to the study of jet correlations for production of one forward and one central jet at the LHC. The case of forward-backward jets will be examined in a forthcoming article. We propose that measurements of hadronic final-state observables associated with forward-central correlations can provide, starting with the data already taken at the LHC, a sensitive probe of how well QCD multiple radiation is taken into account in the Monte Carlo event generators to be used for analyses of experimental data in the forward region. The results of such investigations can serve to estimate the size of backgrounds from QCD radiation between jets at large rapidity separations for Higgs boson searches in vector boson fusion channels.

Besides the contribution of the higher-order radiative corrections taken into account via the results of [17], the need for realistic Monte Carlo simulations of forward particle production raises the question of whether non-negligible effects may come from multiple parton interactions. Such multiple interactions are modeled in parton-shower event generators used for Monte Carlo simulation of final states at the LHC [18–21], and form the subject of a number of current efforts [22–29] to construct approaches capable of describing multiple parton scatterings. In this paper we investigate multi-parton interaction effects for forward-central jet correlations within the model [18, 20]. We observe that, compared to the production of multiple jets in the single-scattering picture [17], the multi-parton mechanism [18, 20] shifts a significant amount of gluon emissions to larger values of the longitudinal momentum fraction x in the initial-state decay chains, because less energy is available to each of the sequential parton chains. This results into differences in the shapes of the forward-central jet correlations in the azimuth and rapidity plane between the single-chain and multiple-chain mechanisms for multi-jet production. This can be investigated at the LHC also via measurements of particle and energy flow associated with forward production: we leave the study of this to future work.

The paper is organized as follows. In Sec. 2 we give a concise discussion of the high-energy QCD dynamics underlying the hadroproduction of forward jets, based on the results of [17]. We describe the high-energy factorized form of the forward jet cross section that is to be coupled to parton showering in order to achieve a full description of the associated

2

hadronic final states. In Sec. 3 we discuss aspects of the initial-state parton showers relevant to forward hadroproduction. In particular we consider a method to implement parton branching at transverse-momentum dependent level not only for gluon-initiated channels in the backwards evolution but also for quark-initiated channels. In Sec. 4 we present results of numerical Monte Carlo calculations for transverse momentum and pseudorapidity spectra and for forward-central correlations in azimuthal angle and pseudorapidity. We compare single versus multiple parton interactions, and propose various measurements of forward jet observables at the LHC. We give concluding remarks in Sec. 5.

2 Hadroproduction of forward jets

This section summarizes results from [17]. In particular we discuss the physical picture underlying the factorization formula that will be used for numerical calculations in later sections.

Consider the hadroproduction of a forward jet associated with a hard final state X, as depicted in Fig. 1. The kinematics of the process is characterized by the large ratio of sub-energies $s_2/s_1 \gg 1$ and highly asymmetric longitudinal momenta in the partonic initial state ($x_A \to 1$, $x_B \to 0$).
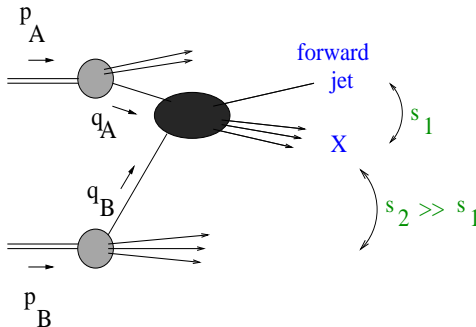

Figure 1: *Jet production in the forward rapidity region in hadron-hadron collisions.*

The presence of multiple large-momentum scales in the LHC forward kinematics [2, 30] implies that realistic phenomenology of hadronic jet final states requires taking into account at higher order both logarithmic corrections in the large rapidity interval (of BFKL type) and logarithmic corrections in the hard transverse momentum (of collinear type). This can be achieved via QCD factorization at fixed transverse momentum [16]. A pictorial representation of QCD radiative contributions in the rapidity and transverse momentum plane is sketched in Fig. 2. Note that k_T-factorization is valid to single-logarithmic accuracy. In particular, it enables one to obtain logarithmically enhanced terms in rapidity that are not associated to any collinear logarithm; conversely, collinear singularities can be taken into account to any logarithmic accuracy [31]. This in contrast with calculations in double-logarithmic approximations.

The different expansions in Fig. 2 correspond to different possible ways of reorganizing the QCD perturbation series. The results of factorization at fixed k_T can be reobtained by going to sufficiently sub-leading orders in either the BFKL expansion or the collinear

expansion [31]. This applies for instance to the transverse-momentum recoil effects in the collinear case [32], and kinematic effects of energy conservation in the BFKL case [33].
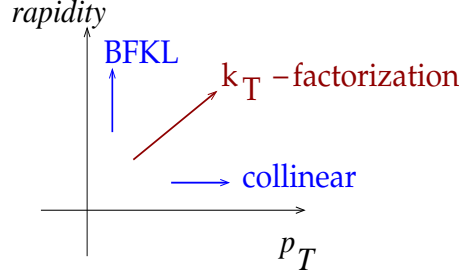

Figure 2: *QCD radiative contributions to forward jet production in the rapidity and transverse momentum plane.*

2.1 Factorization of the jet cross section

Recall that in the case of forward jet leptoproduction [34] QCD factorization at fixed transverse momentum allows one to compute the high-energy asymptotic coefficients for the coupling of forward jets to deeply inelastic scattering [16, 35]. Since the early phenomenological studies [36] forward jet leptoproduction has been investigated at HERA, and will play a major role at the proposed future lepton facilities [37] (LHeC, EIC). We come back to the possible role of lepton analyses in Sec. 5.

In the case of hadroproduction the k_T-factorized form of the forward jet cross section is given in [17]. This is represented schematically in Fig. 3. Initial-state parton configurations contributing to forward jet production are asymmetric, with the parton in the top subgraph being probed near the mass shell and large x, while the parton in the bottom subgraph is off-shell and small-x. The jet cross section differential in the final-state transverse momentum Q_t and azimuthal angle φ is given schematically by

$$\frac{d\sigma}{dQ_t^2 d\varphi} = \sum_a \int \phi_{a/A} \otimes \frac{d\widehat{\sigma}}{dQ_t^2 d\varphi} \otimes \phi_{g^*/B} \ , \tag{1}$$

where $\otimes$ specifies a convolution in both longitudinal and transverse momenta, $\widehat{\sigma}$ is the hard scattering cross section, calculable from a suitable off-shell continuation of perturbative matrix elements [17], $\phi_{a/A}$ is the distribution of parton a in hadron A obtained from near-collinear shower evolution, and $\phi_{g^*/B}$ is the gluon unintegrated distribution in hadron B obtained from non-collinear, transverse momentum dependent shower evolution.

Fig. 4 shows a typical graph contributing to the off-shell matrix element in the qg channel. By parameterizing the exchanged momenta k_1 and k_2 in terms of purely transverse four-vectors k_{T1} and k_T and longitudinal momentum fractions ξ_i and $\overline{\xi}_i$ as

$$p_1 - p_5 = k_1 = \xi_1 p_1 + k_{T1} + \overline{\xi}_1 p_2 \ , \quad p_2 - p_6 = k_2 = \xi_2 p_2 + k_T + \overline{\xi}_2 p_1 \ , \tag{2}$$

the forward kinematics implies [17] $(p_4 + p_6)^2 \gg (p_3 + p_4)^2$, $k_1 \simeq \xi_1 p_1$, $k_2 \simeq \xi_2 p_2 + k_T$, so that

$$p_5 \simeq (1 - \xi_1)p_1 \ , \quad p_6 \simeq (1 - \xi_2)p_2 - k_\perp \ , \quad \xi_1 \gg \xi_2 \ . \tag{3}$$
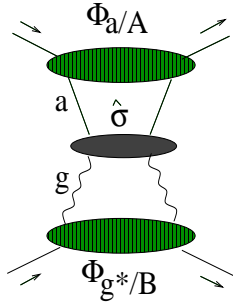
Figure 3: *Factorized structure of the cross section.*

In [17] the full set of the short-distance matrix elements in the forward region, needed for the evaluation of the k_T-factorized jet cross section (1), is computed in exclusive form, for all partonic channels.
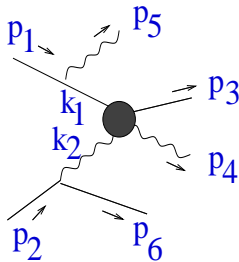

Figure 4: *A typical graph contributing to the off-shell matrix element in the qg channel.*

As discussed in [17], these matrix elements, though not on shell, are gauge invariant and perturbatively calculable. These matrix elements are useful because in the high-energy limit they factorize not only in the collinear emission region but also in the large-angle emission region. As long as the factorization is carried out in terms of distributions for parton splitting at fixed transverse momentum, they can serve to take into account effects of coherence from multi-gluon emission, away from small angles, which become important for correlations among jets across long separations in rapidity. We will exploit this in performing numerical calculations for central + forward jets in Sec. 4.

2.2   Hard matrix elements and merging

The precise behavior in transverse momentum resulting from the finite-angle radiation taken into account by the method described above is illustrated in Fig. 5 [17]. Here we consider the qg channel contribution to forward jet production. (Analogous results for all channels can be found in [17].) We show separately the abelian and non-abelian terms, proportional respectively to the color factors C_F^2 and $C_A C_F$ ($C_F = (N_c^2 - 1)/(2N_c)$, $C_A = N_c$). With reference to Fig. 4, the variables Q_T and φ are the final-state transverse momentum and azimuthal angle defined by

$$Q_T = (1 - \nu)p_{T4} - \nu p_{T3} \;, \quad \text{where} \quad \nu = (p_2\, p_4)/[(p_2\, p_1) - (p_2\, p_5)] \;, \tag{4}$$

$$\cos\varphi = Q_T \cdot k_T / |Q_T||k_T| \quad , \tag{5}$$

while k_T is the transverse momentum defined by Eq. (2), and effectively measures the distribution of the jet system recoiling against the leading di-jets.
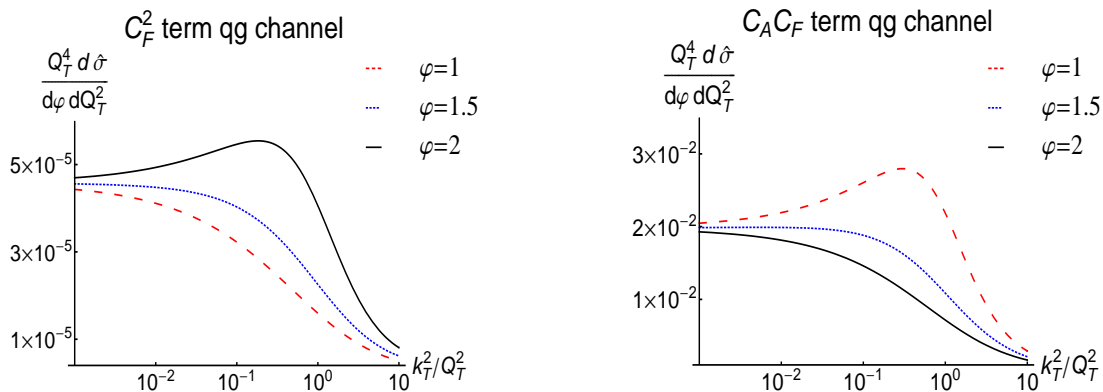

Figure 5: *Transverse momentum dependence of the factorizing short-distance matrix elements.*

The region $k_T / Q_T \to 0$ in Fig. 5 corresponds to the leading-order process, with two back-to-back jets. The result in this region is simply given by the small-angle limit

$$\frac{Q_T^4 d\hat{\sigma}}{dQ_T^2 d\varphi} \to \alpha_s^2 f^{(0)}(p_T^2/s) \quad , \quad Q_T \to p_T = |p_{T3}| = |p_{T4}| \quad , \tag{6}$$

where the function $f^{(0)}$ is given by [17]

$$f^{(0)}(z) = \frac{1}{16\sqrt{1-4z}} \left[C_F^2 z(1+z) + 2C_F C_A(1 - 3z + z^2) \right] \quad . \tag{7}$$

The summation of logarithms for large rapidity $y \sim \ln s/p_T^2$, on the other hand, is achieved by convolution of the k_T cross section in Fig. 5 with unintegrated parton-splitting functions [16]. While in the collinear approximation case the small-angle result in Eqs. (6),(7) is taken to be valid, in leading order, throughout the range of transverse momentum scales up to the factorization scale, we see from the result in Fig. 5 that the role of higher-order, multi-gluon emission at large rapidities is to provide a modulation by setting the dynamical cut-off at values of k_T of order Q_T. The essential point is that non-negligible effects may arise at high energy from the finite-k_T tail. The quantitative evaluation of these effects is obtained by integrating the distribution in Fig. 5 over the initial-state parton showers, also taken to be transverse-momentum dependent (see Sec. 3). We will perform such parton shower calculations explicitly in the next sections.

Observe that, as in any parton shower calculation beyond leading order, in order to combine the hard radiation encoded in the short distance matrix element with the radiation from parton showering one needs a specific scheme for merging the two contributions consistently, by avoiding double counting. The high-energy factorization of Subsec. 2.1 can be viewed as providing precisely such a merging scheme. In particular, we recall from [16, 38]

6

that the convolution of off-shell matrix elements over transverse-momentum dependent parton-splitting functions is carried out by using systematically the relation for the $2 + 1$ jet cross section

$$\int d^2 k_T \left(\frac{1}{k_T^2}\right)_+ \widehat{\sigma}(k_T) = \int d^2 k_T \frac{1}{k_T^2} \left[\widehat{\sigma}(k_T) - \Theta(\mu - k_T) \widehat{\sigma}(0_T)\right] \ , \qquad (8)$$

which provides the necessary small-k_T subtraction.

So in Secs. 3 and 4 we will couple Eq. (1) to parton showers and perform parton shower calculations *in the high-energy merging scheme* for hadronic final states associated with forward jets. These calculations will illustrate quantitatively the significance of contributions with $k_T \simeq Q_T$ in the large-y region, and will be compared with results of collinear-shower generators, which do not include such finite-k_T effects. We note in particular that the dependence on the azimuthal angle shown in Fig. 5 is of direct relevance, as we will see in Sec. 4, for forward-region measurements involving azimuthal plane correlations between jets far apart in rapidity.

It is worth noting that the approach summarized above allows forward jets to be produced either from the hard scatter subprocess or from the parton evolution subprocess. We will see an explicit numerical illustration of this in Sec. 4. This picture can be contrasted with the picture from collinear [10] and BFKL [15] approaches, in which forward jets are produced by hard matrix elements or impact factors. This feature of the present approach can be traced back to the fact that the factorization (1) provides the correct interpolation at high energy between the collinear emission and finite angle regions [16].

Because forward jet production probes the gluon density function for small x (see discussion around Fig. 3), it can naturally be used to investigate possible nonlinear effects [39–41] at high parton density. We do not pursue the study of such effects in the present paper; but we stress that the formulation [17] at fixed transverse momentum is suitable to describe the approach to the high-density region, since, as explained above, it is designed to take into account both the effects from BFKL evolution associated with the increase in rapidity and also the effects from increasing p_T described by renormalization group, which are found to be also quantitatively significant [42–44] for studies of parton saturation. We point the reader to e.g. [45–47] for first Monte Carlo calculations along these lines, and [48] for extension to nucleus-nucleus collisions.

3   Shower evolution and the unintegrated quark density

To obtain a detailed description of the hadronic final states associated with forward jets, we need a full parton-shower calculation. This section describes basic features of the showering algorithm that we use for such calculations.

As noted earlier, the factorization formula in Sec. 2 can be used jointly with parton showering. Because in the forward kinematics one of the longitudinal momentum fractions x in the initial state becomes small, in order to take full account of multi-gluon emission

coherence one needs to keep finite-k_T terms in the initial-state parton branching [49–52].[1] We will include these terms according to the CCFM method [54, 55], in particular including also showering for quark density channels as explained below.[2]

The effect of small-x coherence terms on azimuthal and transverse-momentum jet correlations and jet multiplicities has been studied in [49, 60], focusing on the case of jet lepto-production. It is found that quantitative effects become more significant with decreasing x and decreasing distance in the azimuthal plane between the leading jets. The results [49, 60] suggest that the inclusion of small-x coherence terms in the initial-state shower can be relevant in the case of forward jets at the LHC.[3]

It was noted by numerical calculation in [17, 30] that for realistic phenomenology of forward jets in the LHC kinematics one needs to take into account contributions from both quark-density and gluon-density channels. Since CCFM shower evolution has typically only included gluon-density terms [55], here we describe how we implement quark channels. For the forward jet case that we are interested in, the quark density contributes at fairly large values of x. We will thus focus on the valence quark distribution.[4]

We consider the branching evolution equation at the unintegrated, transverse-momentum dependent level according to

$$
\begin{aligned}
xQ_v(x, k_t, \bar{q}) & = xQ_{v0}(x, k_t, \bar{q}) + \int \frac{dz}{z} \int \frac{dq^2}{q^2} \, \Theta(\bar{q} - zq) \\
& \times \, \Delta_s(\bar{q}, zq) P(z, k_t) \, xQ_v\left(\frac{x}{z}, k_t + (1-z)q, q\right) \; ,
\end{aligned}
\tag{9}
$$

where $\bar{q}$ is the evolution scale. The quark splitting function P is given by

$$
P(z, k_t) \;\; = \;\; \bar{\alpha}_s\left(k_t^2\right) \frac{1 + z^2}{1 - z} \; ,
\tag{10}
$$

with $\bar{\alpha}_s = C_F \alpha_s / \pi$. Note that, unlike the CCFM kernel given in the appendix B of [51], in Eqs. (9),(10) the non-Sudakov form factor is not included, because we only associate this factor to $1/z$ terms. The Sudakov form factor Δ_s is given by

$$
\Delta_s(q_i, z_i q_{i-1}) = \exp\left(-\int_{z_{i-1}^2 q_{i-1}^2}^{q_i^2} \frac{dq^2}{q^2} \int_0^{1 - Q_0/q} \frac{1}{1 - z} \, \bar{\alpha}_s(q^2(1-z)^2) \, dz \right) \; .
\tag{11}
$$

Here the fractional energy of the exchanged quark i is given by x_i, and the energy transfer between the exchanged quarks $i - 1$ and i is given by $z_i = x_i / x_{i-1}$. The term xQ_{v0} in

---

[1]This brings in so-called unintegrated, or transverse-momentum dependent, parton distributions. General issues on these distributions are now actively investigated by many authors, and will influence the use of parton branching methods. We comment on this in Sec. 5. More comments may be found in [49, 53].

[2]Alternative methods for taking into account finite-k_T terms in the parton shower are considered in [56–58]. See [53, 59] for overviews of the subject.

[3]Effects similar to those computed in [49] may also affect azimuthal distributions of b jets [61, 62] and jet multiplicities associated with Higgs boson production [63]. Early measurements of forward jets at the LHC can be helpful in this respect to test how well initial state radiation is described and/or for the QCD tuning of Monte Carlo event generators. For the counterpart of this in the case of central jets see the first LHC measurements [64, 65].

[4]Work to treat the sea quark distribution at unintegrated level is underway [66].

Eq. (9) is the contribution of the non-resolvable branchings between starting scale q_0 and evolution scale $\bar{q}$, given by

$$xQ_{v0}(x, k_t, \bar{q}) = xQ_{v0}(x, k_t, q_0)\Delta_s(\bar{q}, q_0) \ , \tag{12}$$

where Δ_s is the Sudakov form factor, and the starting distributions at scale q_0 are parameterized using the CTEQ5 u and d valence quark distributions [67] as

$$xQ_{v0}(x, k_t, q_0) = xQ_{v\,\mathrm{CTEQ}}(x, q_0) \ \exp[-k_t^2/\lambda^2] \ , \tag{13}$$

with $\lambda = 0.92 \ GeV$.

We next solve Eq. (9) numerically. In fig. 6(left) the unintegrated u-quark and d-quark distributions are shown as a function of x and as a function of k_t. In fig. 6(right) we show the following integral of the quark distribution

$$\int_0^{\bar{q}} xQ_v(x, k_t, \bar{q}) \ dk_t \ , \tag{14}$$

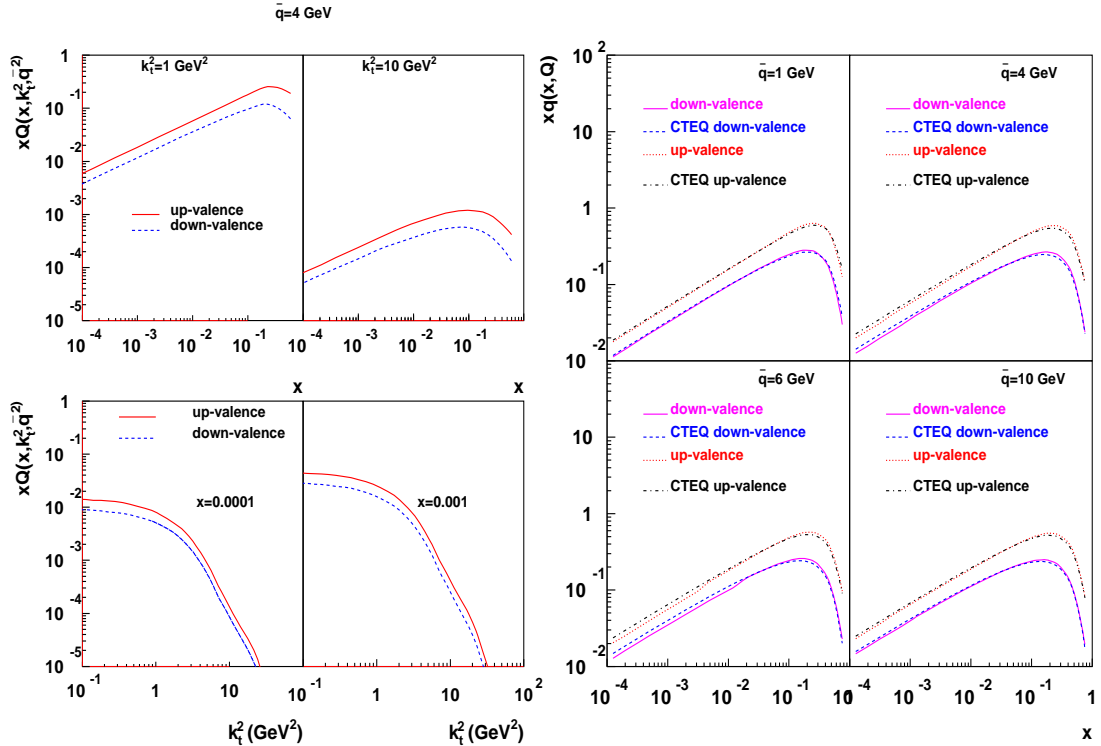and compare this for consistency with the distribution obtained from CTEQ [67] at the same scale.

Figure 6: *Left: Unintegrated quark distribution (u, d-quarks) as a function of x at fixed k_t (top) and as a function of k_t at fixed x (bottom) at a scale $\bar{q} = 4$ GeV. Right: Integral of the unintegrated quark distribution (u, d-quarks) as a function of x for different scales $\bar{q}$. Also shown is the u, d-quark distribution obtained from CTEQ [67].*

9

4   Central + forward jet production at the LHC

In a typical LHC experiment jets can be measured for high transverse energy $E_\perp > 30$ GeV in a large range of pseudorapidity η. In the following we consider differential cross sections for dijets (Fig. 7) reconstructed with the Siscone algorithm [68] with $R = 0.4$, where one jet is in the central region defined by $|\eta_c| < 2$ and the other jet is in the forward region defined by $3 < |\eta_f| < 5$.
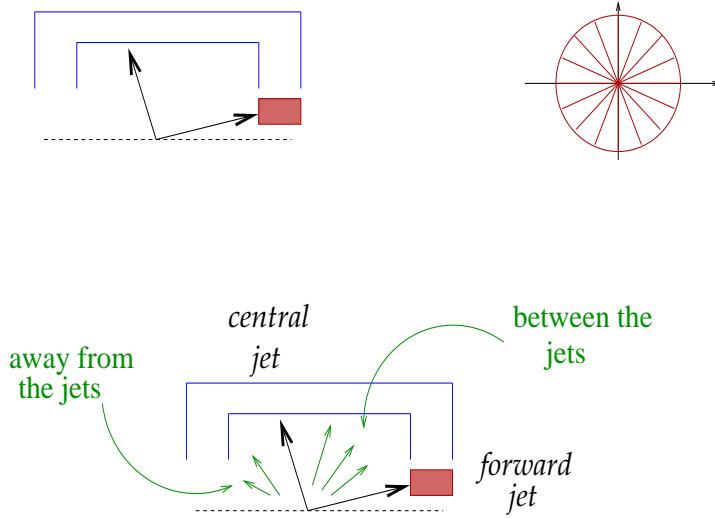

Figure 7: *(top) Jets in the forward and central detectors, and azimuthal plane segmentation; (bottom) particle and energy flow in the inter-jet and outside regions.*

4.1   Dijet cross section and ΔR distribution

The total cross section for a central and a forward jet obtained with the CASCADE [54] Monte Carlo event generator (version 2.2.03 including the matrix element calculated in [17], the unintegrated gluon distribution **set A** and the unintegrated valence quark distribution described in section 3) is given in Tab. 1. We compare the prediction from CASCADE with the prediction from the PYTHIA [20] Monte Carlo event generator running in two modes: with and without multi-parton interactions (Fig. 8). We use tune P1 [18], which allows for more radiation from parton shower. Both Monte Carlo generators simulate higher order QCD corrections with parton showers: CASCADE uses parton showers according to the CCFM evolution equation whereas PYTHIA uses DGLAP based parton showers. The total cross section predicted by CASCADE lies in between the prediction of PYTHIA with and without multiparton interactions (Tab. 1).

In Fig. 9 we investigate the physical mechanism producing the central and forward jets. We plot $\Delta R = \sqrt{(\Delta\phi)^2 + (\Delta\eta)^2}$, where $\Delta\phi = \phi_{jet} - \phi_{part}$ ($\Delta\eta = \eta_{jet} - \eta_{part}$) is the azimuthal (pseudorapidity) difference between the jet and the corresponding parton
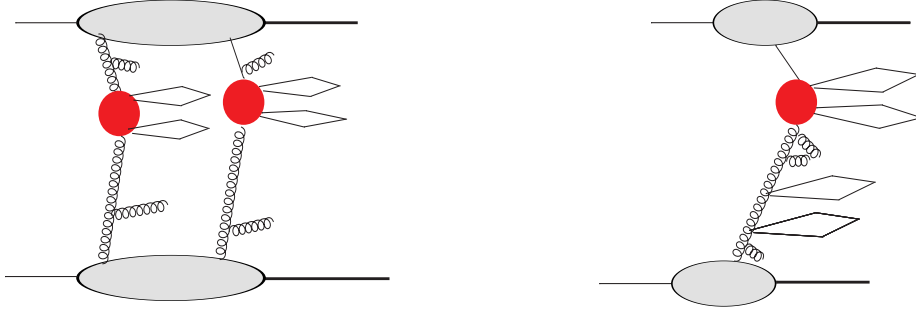
Figure 8: *Multi-jet production by (left) multiple parton chains; (right) single parton chain.*

Table 1: *Integrated dijet cross section for $E_T > 10(30)$ GeV in the range $|\eta_c| < 2$ and $3 < |\eta_f| < 5$.*

	$\sigma(E_T > 10\ GeV)$	$\sigma(E_T > 30\ GeV)$
CASCADE	469 μb	3.1 μb
PYTHIA (MPI) (P1)	798 μb	3.5 μb
PYTHIA (no MPI)	346 μb	3.3 μb

from the matrix element. The ΔR distribution allows one to see whether the jets are dominated by hard partons from the matrix element, or whether they originate from the parton shower. For the low E_T jets the distribution in ΔR has a significant contribution from jets not corresponding to a parton from the matrix element ($\Delta R > 1$).

The bump structure of the distribution at $\Delta R > 1$ is consistent with random distributions in $\Delta\phi$ and $\Delta\eta$ within the phase space region investigated here, showing that indeed $\Delta R > 1$ corresponds to the region where there is no correlation between the parton from the matrix element and the jet.

It is interesting to observe that CASCADE predicts a similar distribution as obtained from PYTHIA with multiparton interactions, whereas PYTHIA without multiparton interactions has a significantly smaller contribution at large ΔR. The situation changes for the high E_T jets: CASCADE predicts significantly more jets (especially in the central region) coming from the parton shower as compared to PYTHIA. This behavior is understandable, as the small-x initial-state parton shower allows for higher transverse momentum radiation compared to a collinear parton shower. It also shows, that the most forward jet is mainly coming from the matrix element parton, whereas the central jet has a significant contribution from the parton shower.

4.2 Transverse momentum spectra

Figs. 10 and 11 show the differential cross section $d\sigma/dE_T$ for jets reconstructed with the Siscone algorithm in the central region defined by $|\eta_c| < 2$ and in the forward region defined
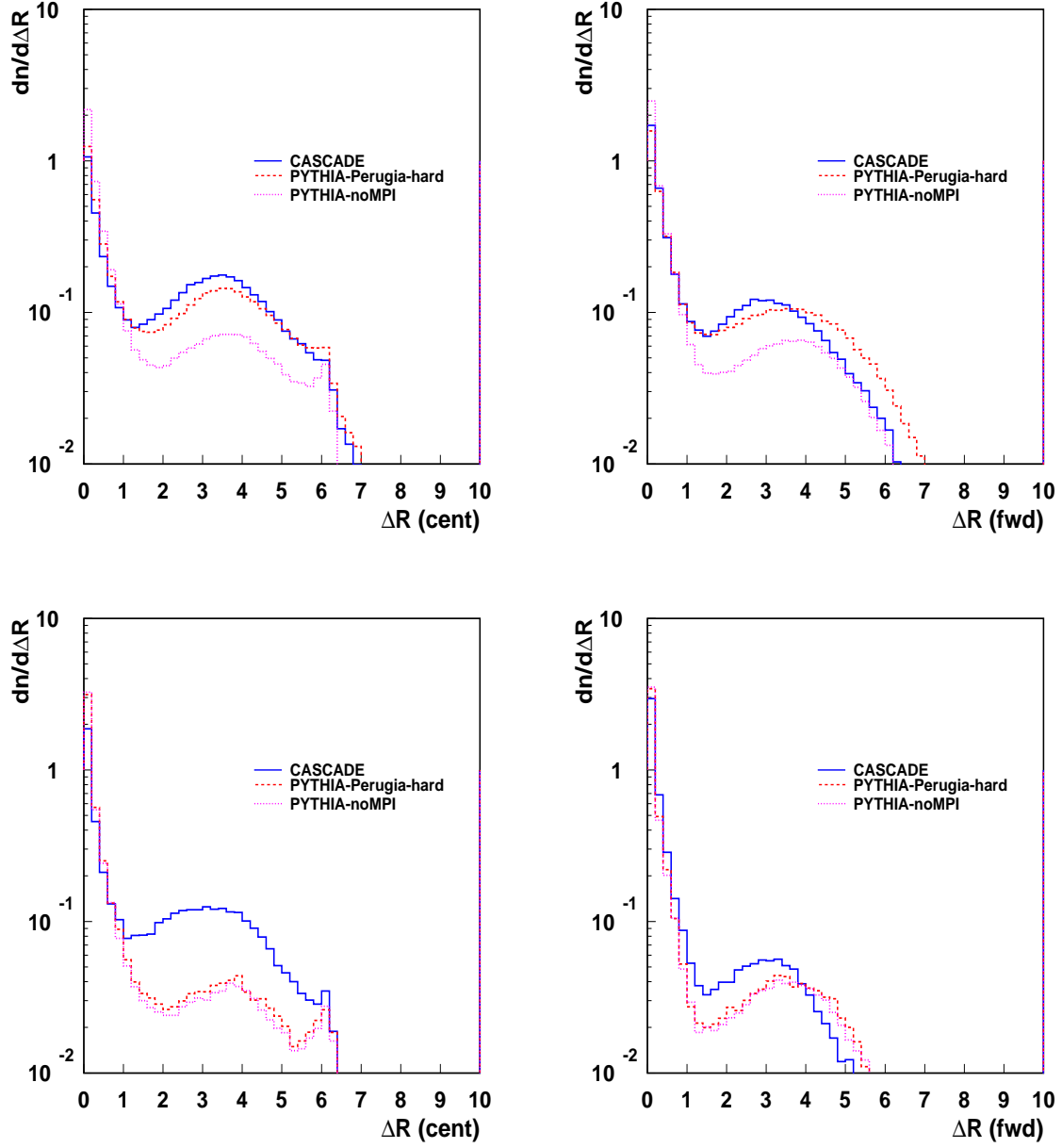
Figure 9: ΔR distribution of the central ($|\eta_c| < 2$, left) and forward jets ($3 < |\eta_f| < 5$, right) for $E_T > 10$ GeV (upper row) and $E_T > 30$ GeV (lower row). The prediction from the $k_\perp$ shower (CASCADE) is shown with the solid blue line; the prediction from the collinear shower (PYTHIA) including multiple interactions and without multiple interactions is shown with the red and purple lines.

by $3 < |\eta_f| < 5$. The left(right) plots show the results when both jets have $E_T > 10(30)$ GeV. We see that the $k_\perp$-dependent parton shower implemented in CASCADE produces a significantly harder spectrum especially for the jet in the central region when both jets are required to have $E_T > 10$ GeV. The predictions from PYTHIA with and without multiparton interactions are similar at large E_T, whereas the multiparton interactions contribute significantly in the low E_T region ($E_T < 30$ GeV) resulting in a larger cross section.
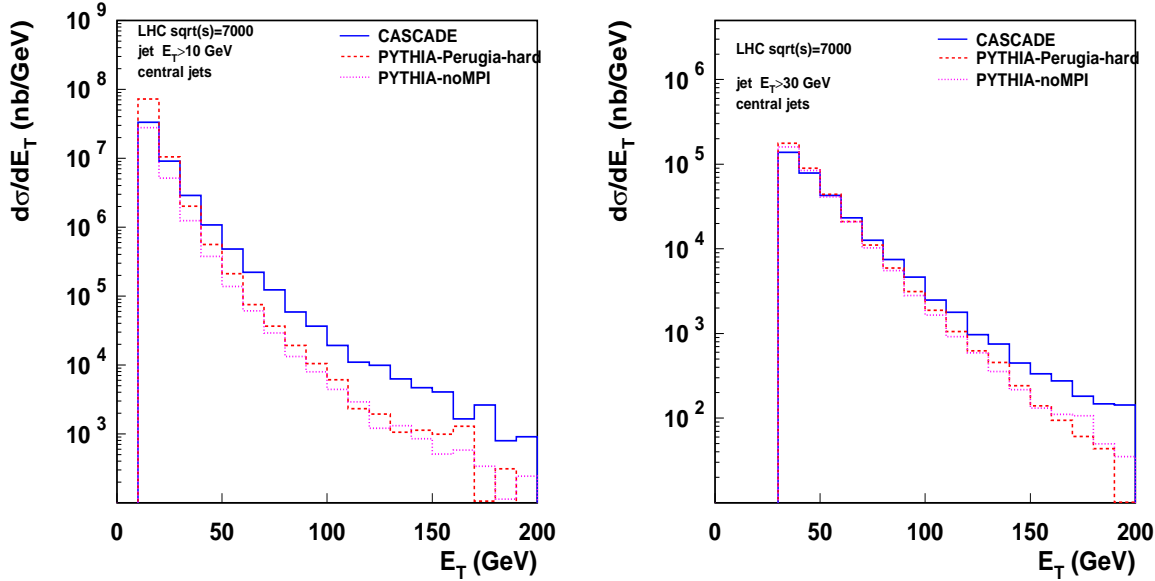

Figure 10: *Transverse momentum spectra of central jets with $|\eta_c| < 2$ at $\sqrt{s} = 7$ TeV for $E_T > 10$ GeV (left) and for $E_T > 30$ GeV (right) for events which have a forward jet with $E_T > 10(30)$ GeV in $3 < |\eta_f| < 5$. The prediction from the $k_\perp$ shower (CASCADE) is shown with the solid blue line; the prediction from the collinear shower (PYTHIA) including multiple interactions and without multiple interactions is shown with the red and purple lines.*

This behavior can be understood since CASCADE uses matrix elements which are calculated within high-energy factorization, allowing harder transverse momentum dependence as compared to collinear factorization. Moreover CASCADE uses the CCFM parton shower with angular ordering which at small x allows for a random walk in transverse momentum, and thus allows for more and harder parton radiation compared to DGLAP based parton shower as implemented in PYTHIA.

It is also interesting to observe that the contribution from multiparton interactions as implemented in PYTHIA is important only for the region of low E_T jets. We have checked also the prediction obtained from PYTHIA using a different parameter set for the modeling of multiple-parton chains (tune D6T [19]). We find that the difference between the different tunes for the multiparton interaction parameters is smaller than the difference coming from the noncollinear corrections to single-chain parton shower.

To see better the significance of the results in Figs. 10 and 11, we have also considered the next-to-leading-order Monte Carlo generator POWHEG [69]. We find that the E_T spectra
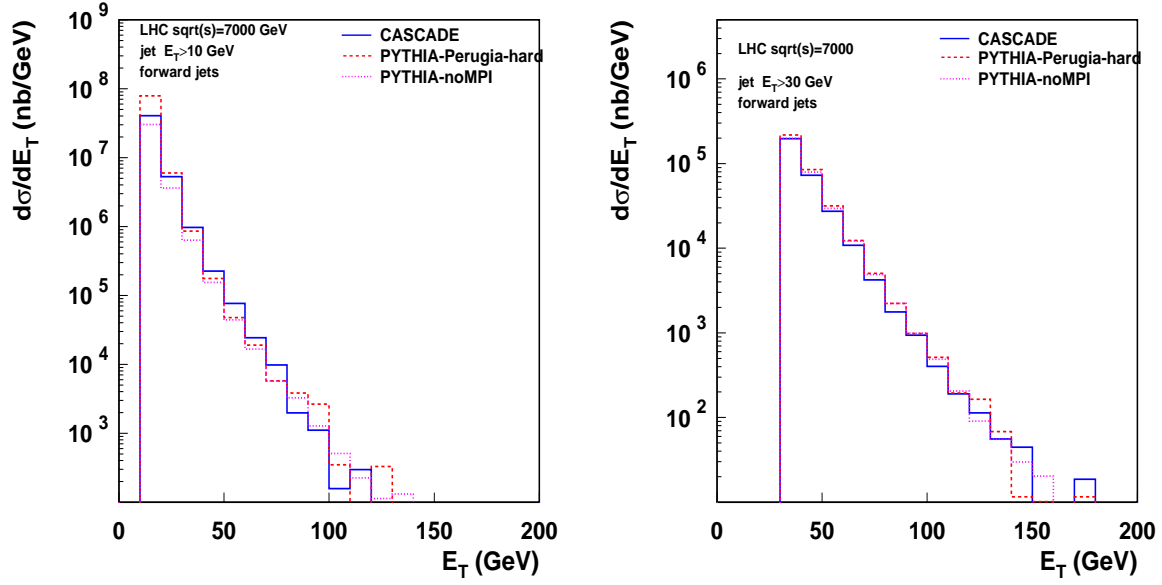
Figure 11: *Transverse momentum spectra of forward jets with $3 < |\eta_f| < 5$ at $\sqrt{s} = 7$ TeV for $E_T > 10$ GeV (left) and for $E_T > 30$ GeV (right) for events which have a forward jet with $p_\perp > 10(30)$ GeV in $|\eta_c| < 2$. The prediction from the $k_\perp$ shower (CASCADE) is shown with the solid blue line; the prediction from the collinear shower (PYTHIA) including multiple interactions and without multiple interactions is shown with the red and purple lines.*

from POWHEG, in the range of rapidity and transverse energy considered here, are very close to those of PYTHIA, indicating that the enhancement from the $k_\perp$ shower in Figs. 10 and 11 is not simply due to the next-to-leading term, but comes from corrections beyond next-to-leading order. This feature is noteworthy; its study should be extended to a wider range of forward-jet observables.
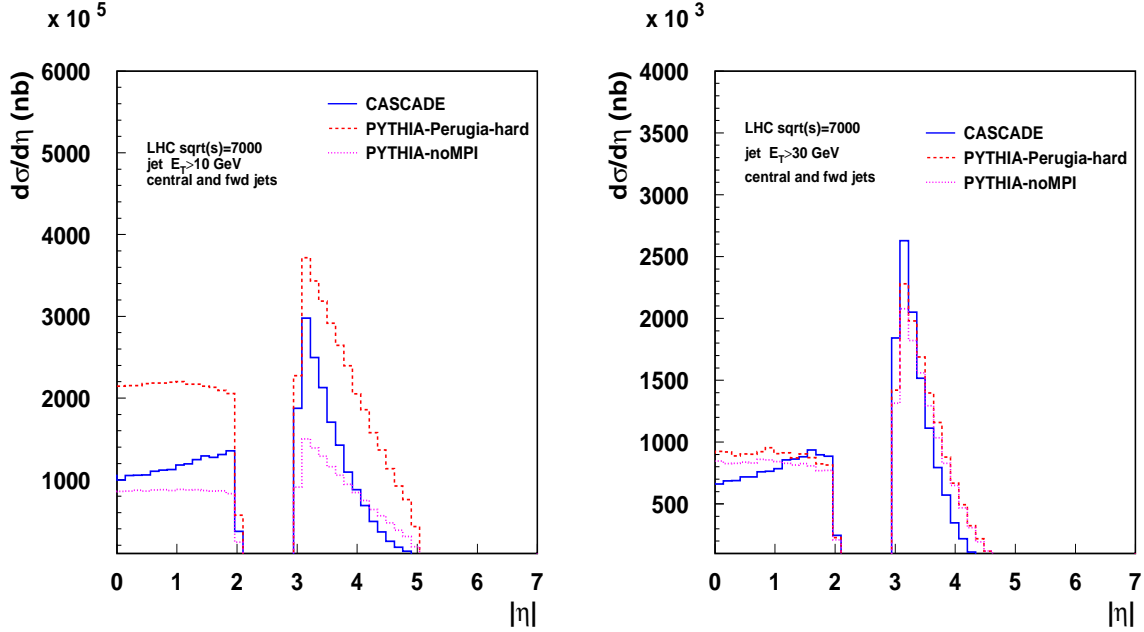
4.3 Rapidity dependence

Figure 12: *Pseudorapidity spectra of produced jets for $\sqrt{s} = 7\,TeV$ with requirement that $p_T > 10\,GeV$ (left) and $p_T > 30\,GeV$ (right). CASCADE is shown with the blue solid line, PYTHIA with (without) multiparton interactions is shown as the dashed red (dotted purple) line.*

In Fig. 12 we show the differential cross section $d\sigma/d\eta$ for dijet events with $E_T > 10(30)$ GeV in two regions of $0 < |\eta| < 2$ and $3 < |\eta| < 5$. Again we compare the prediction from CASCADE with the one from PYTHIA without and with multiparton interactions.

We observe that the cross section in the central region for CASCADE is rising towards larger η whereas for PYTHIA the cross section is flat. The cross section in the forward region is steeply falling towards large η. The slope of this distribution is different from CASCADE and PYTHIA. A closer investigation of these different behaviors is underway. A significant contribution to the difference comes from the treatment of the quark distribution (Sec. 3), and suggests the need to include both valence and sea quark distributions at unintegrated level.

From Fig. 12 (left) we see that at small E_T the influence from multiparton interactions in PYTHIA is significant. CASCADE predicts a cross section of similar size as PYTHIA with multiparton interactions in the region $3 < \eta < 3.5$, but the distribution falls more rapidly towards larger η. In the large E_T region (Fig. 12 (right)) the differences in cross sections as a function of η become smaller.

4.4 Azimuthal dependence

The azimuthal correlation of a central and forward jet is a measure of the parton radiation between the jets and is therefore a probe of how well the Monte Carlo parton shower is simulating the higher-order parton emissions. The azimuthal decorrelation of forward and backward jets has been proposed as one of the measurements to test BFKL dynamics [15](and references therein). In lowest order, BFKL predicts a much larger decorrelation compared to calculations in collinear factorisation. With a larger separation of the jets in $\Delta\eta$, the phase space for parton radiation is increased. However, significant multiparton interactions could perhaps mimic a signal expected from small x dynamics.

In Fig. 13 we show the differential cross section $d^2\sigma/d\Delta\phi\Delta\eta$. The decorrelation as a function of $\Delta\eta$ increases in CASCADE as well as in PYTHIA. In the low E_T region (Fig. 13 (left)) the increase in decorrelation with increasing $\Delta\eta$ is very significant. The cross section for jet separation up to $\Delta\eta < 4$ is very similar between CASCADE and PYTHIA with multiparton interactions, whereas a clear difference is seen to PYTHIA without multiparton interactions. However, at large $\Delta\eta > 4$ the decorrelation predicted by CASCADE is significantly larger than the prediction including multiparton interactions.

In the higher E_T region CASCADE predicts everywhere a larger decorrelation. In this region, the influence of multiparton interactions in PYTHIA is small and the difference to CASCADE comes entirely from the different parton shower.

In Fig 14 we show the average $\langle\cos(\Delta\phi - \pi)\rangle$ as a function of the rapidity separation $\Delta\eta$ of the central and forward jets. This quantity is considered in [10, 13–15] as a sensitive probe for BFKL dynamics. We observe that the distribution of $\langle\cos(\Delta\phi - \pi)\rangle$ at $p_T > 10\,GeV$ shows only little difference between CASCADE and PYTHIA, whereas the differential distribution of $d^2\sigma/d\Delta\phi\Delta\eta$ (Fig. 13) is more discriminative. In the $p_T > 30\,GeV$ case CASCADE predicts a larger decorrelation than PYTHIA, consistent with what is observed in Fig. 13.

5 Summary and outlook

The production of hadronic jets in the forward region of pp collisions will form a largely new area of experimental and theoretical activity at the Large Hadron Collider. Forward jet production will enter the LHC physics program both for new particle discovery processes (e.g., vector boson fusion channels for Higgs boson searches) and for new aspects of standard model physics (e.g., QCD at small x and its interplay with cosmic ray physics).

In this paper we have focused on the study of jet correlations for production of a forward and a central jet at the LHC. The capabilities of LHC forward and central detectors allow measurements of such correlations to be made for the first time across large rapidity intervals ($\Delta y \gtrsim 4 \div 6$). In this kinematic region the evaluation of QCD theoretical predictions is made complex by the presence of multiple mass scales, which raises questions on the potential need for, on one hand, perturbative QCD resummations and, on the other hand, possible corrections beyond single parton scattering.

To address the structure of the final states associated with forward jet production, in this paper we have used a merging scheme based on high energy factorization [16, 17] to combine hard matrix elements and parton showering. This is designed to incorporate

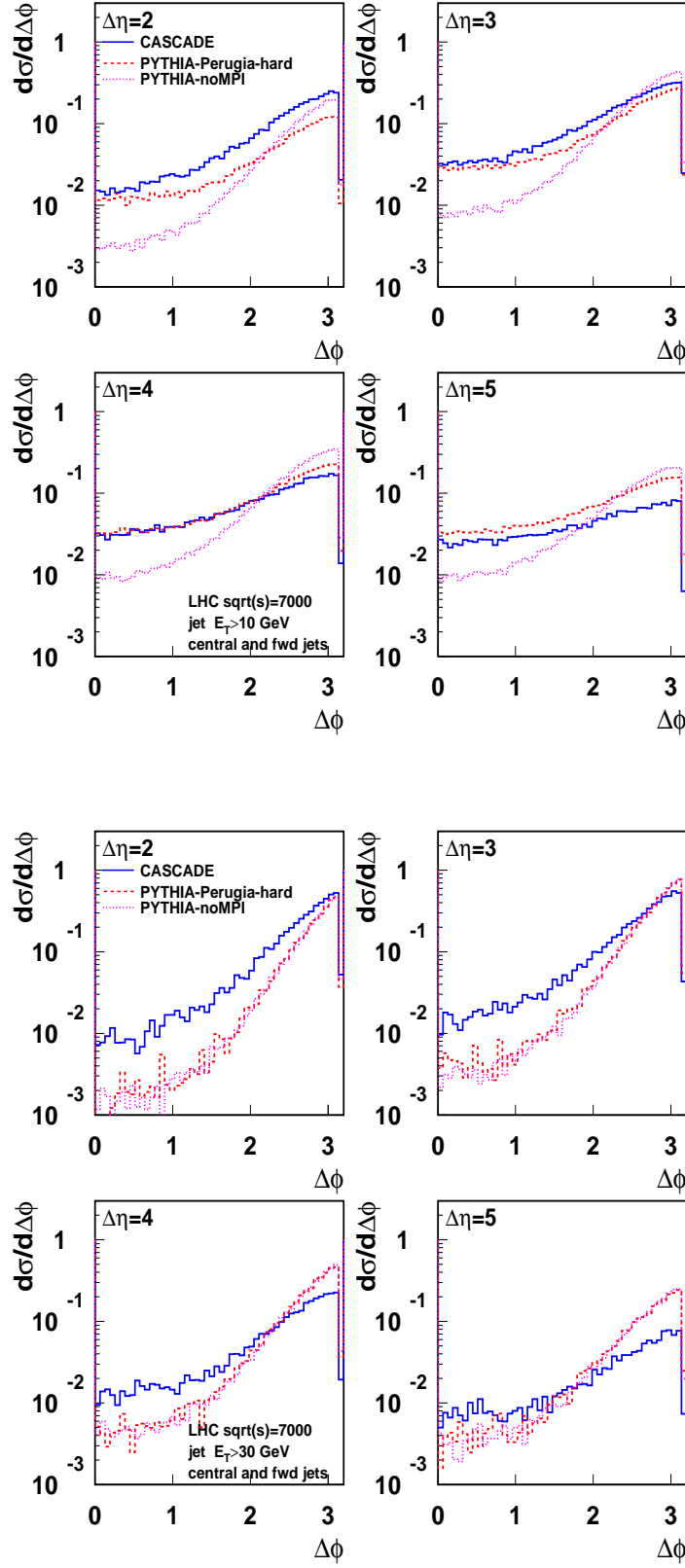Figure 13: *Cross section as a function of the azimuthal difference $\Delta\phi$ between the central and the forward jet for different separations in pseudorapidity $\Delta\eta$, at $\sqrt{s} = 7\,TeV$ for jets with $p_T > 10\,GeV$ (upper) and $p_T > 30\,GeV$ (lower). CASCADE is shown with the blue solid line, PYTHIA with (without) multiparton interactions is shown as the dashed red (dotted purple) line.*
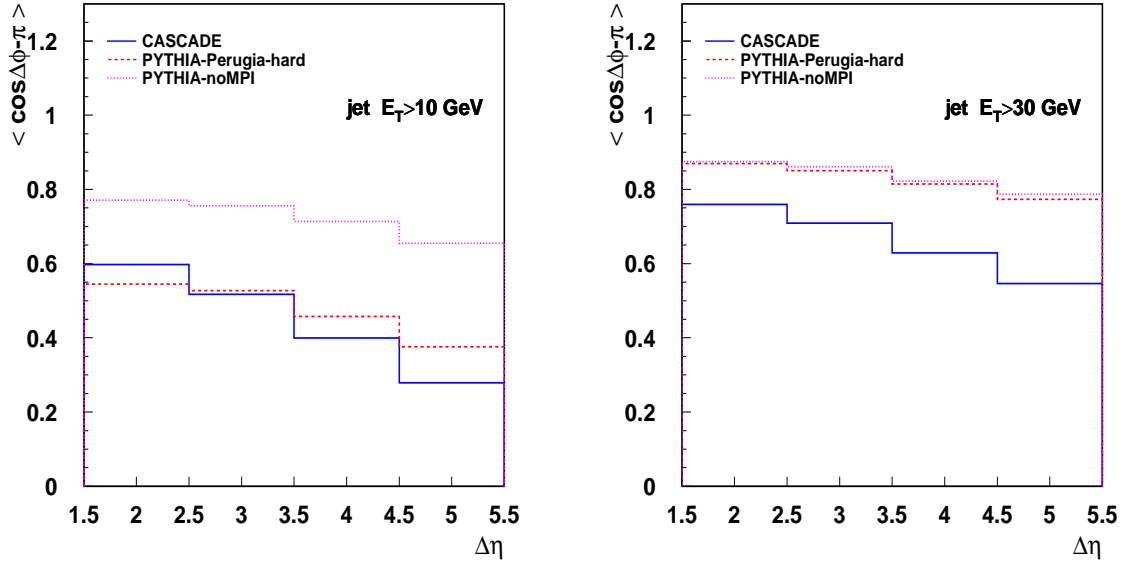
17

Figure 14: *Average* $\langle\cos(\Delta\phi - \pi)\rangle$ *between the central and the forward jet as a function of separation in pseudorapidity* $\Delta\eta$, *at* $\sqrt{s} = 7\,TeV$ *for jets with* $p_T > 10\ GeV$ *(left) and* $p_T > 30\ GeV$ *(right).* CASCADE *is shown with the blue solid line,* PYTHIA *with (without) multiparton interactions is shown as the dashed red (dotted purple) line.*

radiative contributions in such a manner that both logarithmic corrections in the large rapidity interval and logarithmic corrections in the hard transverse momentum are taken into account to higher orders in α_s. Both kinds of contributions are likely to be needed for reliable phenomenology of forward hard production. Their summation is achieved by including finite-k_T terms in the parton branching and matrix elements.

In this approach forward jets may be produced from either the hard scatter subprocess or the parton showering subprocess. The resulting physical picture of forward hard production is thus different from that of purely BFKL or collinear calculations, in which, also at the next-to-leading order (see e.g. [10, 15]), forward jets are produced by hard impact factors or matrix elements.

We have implemented the high-energy merging scheme in the hadron-level shower Monte Carlo event generator CASCADE [54], and used this to obtain numerical predictions for several forward-jet observables. In doing this, we have also implemented in the Monte Carlo generator [54] an algorithm to include the parton branching evolution for the valence quark distribution at unintegrated level, which extends the previous CCFM algorithm [55] for the unintegrated gluon distribution.

We have examined the effects of the higher-order radiative contributions taken into account by this approach by computing the jet transverse-momentum and rapidity spectra and the jet correlations in rapidity and azimuth. We find that the effects are significant especially in the slope of the E_T spectrum and in the jet angular correlations. In particular, we find that while the average cosine of the azimuthal separation between the leading jets is not affected very much as a function of rapidity by finite-k_T terms, the detailed shape of

the $\Delta\phi$ distribution is.

We have also investigated the model [18, 20] for multiple parton interactions, corresponding to corrections beyond single parton scattering. Our analysis shows that certain features of forward jet production such as rapidity and E_T spectra, found by including high-energy, noncollinear corrections to single-chain parton showers, can be mimicked by effects of multiple parton chains. However, distinctive shapes are found both in the ΔR distribution and in the azimuthal correlations. We suggest that measurements of the particle and energy flow in the region both between the jets and away from the jets should have stronger discriminating power between the single-chain and multiple-chain mechanisms for multi-jet production. The detailed analysis of this point will be the subject of a separate paper. Note that this also points to the phenomenological relevance of energy flow observables such as those investigated in [70–72].

As observed in Secs. 2 and 3, many of the theoretical tools that underlie forward jet physics, from parton branching beyond leading order to perturbative QCD resummations to, possibly, the approach to the saturation region, depend on the notion of transverse momentum dependent, or unintegrated, parton distribution functions (u-pdfs). In the calculations of this paper we take the high-energy definition of u-pdfs [16], namely, we rely on the fact that for small x u-pdfs can be defined gauge-invariantly (and can be related to the ordinary pdfs renormalized in the minimal subtraction scheme $\overline{\text{MS}}$ [73]) by going to the high-energy pole in physical amplitudes [16]. More general characterizations of u-pdfs, valid over the whole phase space, are very desirable. A complete framework is yet to be fully developed though. Recent results in this area, see e.g. [74–80], are likely to eventually have a bearing on forward jet physics.

Note that forward hard production processes will be relevant not only for LHC physics but also for physics at the planned future lepton facilities [37] (LHeC, EIC). Thus a unified understanding in hadron-hadron and lepton-hadron collisions is desirable. As recalled in Sec. 2, QCD high-energy factorization [16] has been used to determine the asymptotic coefficients [35] that couple forward jets to deeply inelastic scattering. Since the early phenomenological studies [36], forward jet leptoproduction has been investigated at HERA. Measurements of forward jet cross sections at HERA [81] have illustrated that neither fixed-order next-to-leading calculations nor standard shower Monte Carlo generators [12, 81, 82], e.g. PYTHIA or HERWIG, are able to describe forward jet ep data. This provides additional motivation for developing methods capable of treating the multi-scale kinematics and describing jet production beyond the central rapidity region. It is of interest to analyze HERA data [83] looking at forward + central jets, similarly to what is done in this paper (Sec. 4) for pp collisions; but due to the phase space available for multiple jet radiation, such studies are likely to prove much more relevant at a future high-energy lepton collider.

The analysis performed in this paper shows that the final states associated with forward jet production at the LHC receives significant contributions from radiative corrections that take into account both large logarithms of rapidity and large logarithms of transverse momentum. Distinctive effects are found, for instance, for the distribution in the azimuthal separation $\Delta\phi$ between forward and central jets. We obtain distinctive predictions both with respect to parton showers modeling multiple parton interactions and with respect to parton showers including next-to-leading fixed-order corrections. This analysis can be extended to correlations of forward and backward jets. It can thus serve to estimate the

size of backgrounds from QCD radiation in new particle searches from vector boson fusion channels.

References

[1] M. Grothe, arXiv:0901.0998 [hep-ex].

[2] Z. Ajaltouni et al., arXiv:0903.3861 [hep-ph].

[3] D. d'Enterria, arXiv:0911.1273 [hep-ex].

[4] M. Vazquez Acosta [on behalf of CMS Coll.], arXiv:0901.3098 [hep-ex].

[5] K.J.C. Leney [on behalf of ATLAS Coll.], arXiv:0810.3144 [hep-ex].

[6] M.G. Albrow, T.D Coughlin and J.R. Forshaw, arXiv:1006.1289 [hep-ph].

[7] L.A. Harland-Lang et al., arXiv:1005.0695 [hep-ph].

[8] S. Heinemeyer et al., arXiv:1009.2680 [hep-ph].

[9] R. Engel, in Proceedings of the 30th International Cosmic Ray Conference, ed. R. Caballero et al., vol. 6, p. 359 (Mexico City, 2009).

[10] P. Aurenche, R. Basu and M. Fontannaz, Eur. Phys. J. C **57** (2008) 681; M. Fontannaz, LPT-Orsay preprint 09-86 (April 2009).

[11] A.H. Mueller and H. Navelet, Nucl. Phys. B**282** (1987) 727.

[12] C. Ewerz, L.H. Orr, W.J. Stirling and B.R. Webber, J. Phys. G**26** (2000) 696; J. Forshaw, A. Sabio Vera and B.R. Webber, J. Phys. G**25** (1999) 1511.

[13] L.H. Orr and W.J. Stirling, Phys. Lett. B**436** (1998) 372.

[14] A. Sabio Vera and F. Schwennsen, Nucl. Phys. B**776** (2007) 170; C. Marquet and C. Royon, Phys. Rev. D**79** (2009) 034028.

[15] D. Colferai, F. Schwennsen, L. Szymanowski and S. Wallon, JHEP **1012** (2010) 026; arXiv:1010.0160 [hep-ph].

[16] S. Catani, M. Ciafaloni and F. Hautmann, Phys. Lett. B**242** (1990) 97; Nucl. Phys. B**366** (1991) 135.

[17] M. Deak, F. Hautmann, H. Jung and K. Kutak, JHEP **0909** (2009) 121.

[18] P.Z. Skands, arXiv:1005.3457 [hep-ph]; arXiv:0905.3418 [hep-ph], in Proceedings 1st MPI Workshop (Perugia, 2008), DESY-PROC-2009-06, eds. P. Bartalini and L. Fanò.

[19] R.D. Field, in Proceedings 1st MPI Workshop (Perugia, 2008), DESY-PROC-2009-06, eds. P. Bartalini and L. Fanò.

[20] T. Sjöstrand, S. Mrenna, and P. Skands, JHEP **0605** (2006) 026.

[21] M. Bähr, S. Gieseke and M. Seymour, JHEP **0807** (2008) 076.

[22] B. Blok, Yu. Dokshitzer, L. Frankfurt and M. Strikman, arXiv:1009.2714 [hep-ph].

[23] M. Strikman and W. Vogelsang, arXiv:1009.6123 [hep-ph].

[24] T.C. Rogers and M. Strikman, Phys. Rev. D**81** (2010) 016013.

[25] G. Calucci and D. Treleani, arXiv:1009.5881 [hep-ph]; G. Calucci, talk at the ISMD 2010 Symposium (Antwerp, September 2010).

[26] S. Domdey, H.-J. Pirner and U.A. Wiedemann, Eur. Phys. J. C **65** (2010) 153.

[27] E. Maina, arXiv:1010.5674 [hep-ph]; JHEP **0909** (2009) 081; JHEP **0904** (2009) 098.

[28] E.L. Berger, C.B. Jackson and G. Shaughnessy, Phys. Rev. D**81** (2010) 014014; E.L. Berger, talk at ICHEP 2010 (Paris, July 2010).

[29] J.R. Gaunt and W.J. Stirling, JHEP **1003** (2010) 005; J.R. Gaunt, C.-H. Kom, A. Kulesza and W.J. Stirling, Eur. Phys. J. C **69** (2010) 53.

[30] M. Deak et al., arXiv:0908.1870 [hep-ph]; F. Hautmann, arXiv:0909.1250 [hep-ph].

[31] S. Catani and F. Hautmann, Nucl. Phys. B**427** (1994) 475; Phys. Lett. B**315** (1993) 157.

[32] J.C. Collins and H. Jung, hep-ph/0508280.

[33] J.R. Andersen et al, Eur. Phys. J. C **48** (2006) 53.

[34] A.H. Mueller, Nucl. Phys. B Proc. Suppl. **18C** (1990) 125.

[35] S. Catani, M. Ciafaloni and F. Hautmann, Nucl. Phys. B Proc. Suppl. **29A** (1992) 182.

[36] J. Kwiecinski, A.D. Martin and P.J. Sutton, Phys. Rev. D**46** (1992) 921; J. Bartels, A. De Roeck and M. Loewe, Z. Phys. **C54** (1992) 635; W.K. Tang, Phys. Lett. B**278** (1992) 363.

[37] P. Laycock et al., "Future of DIS" summary report, in Proceedings of the Workshop DIS 2010 (Florence, April 2010).

[38] S. Catani, M. Ciafaloni and F. Hautmann, in Proceedings of the Workshop "Physics at HERA", Hamburg 1991, vol. 1, p. 690.

[39] E. Iancu, M.S. Kugeratski and D.N. Triantafyllopoulos, Nucl. Phys. A**808** (2008) 95; E. Iancu, C. Marquet and G. Soyez, Nucl. Phys. A **780** (2006) 52; C. Marquet and R. B. Peschanski, Phys. Lett. B **587** (2004) 201.

[40] Y. Hatta, E. Iancu and A.H. Mueller, JHEP **0801** (2008) 026.

[41] F. Gelis, T. Lappi and R. Venugopalan, Int. J. Mod. Phys. E**16** (2007) 2595.

[42] W.A. Horowitz and Yu.V. Kovchegov, arXiv:1009.0545 [hep-ph].

[43] Yu.V. Kovchegov and H. Weigert, Nucl. Phys. A **807** (2008) 158.

[44] E. Gardi, J. Kuokkanen, K. Rummukainen and H. Weigert, Nucl. Phys. A **784** (2007) 282.

[45] H. Jung and K. Kutak, arXiv:0812.4082 [hep-ph].

[46] E. Avsar and A.M. Stasto, JHEP **1006** (2010) 112.

[47] E. Avsar and E. Iancu, Nucl. Phys. A **829** (2009) 31.

[48] F. Gelis, T. Lappi and R. Venugopalan, Phys. Rev. D**78** (2008) 054019.

[49] F. Hautmann and H. Jung, JHEP **0810** (2008) 113.

[50] G. Marchesini and B.R. Webber, Nucl. Phys. **B386** (1992) 215.

[51] S. Catani, F. Fiorani, and G. Marchesini, Nucl. Phys. **B336** (1990) 18.

[52] M. Ciafaloni, Nucl. Phys. **B296** (1988) 49.

[53] F. Hautmann and H. Jung, Nucl. Phys. Proc. Suppl. **184** (2008) 64 [arXiv:0712.0568 [hep-ph]]; arXiv:0808.0873 [hep-ph].

[54] H. Jung et al., Eur. Phys. J. C **70** (2010) 1237 [arXiv:1008.0152 [hep-ph]].

[55] H. Jung, Comput. Phys. Commun. **143** (2002) 100.

[56] S. Jadach, A. Kusina, M. Skrzypek and M. Slawinska, arXiv:1004.4131 [hep-ph]; arXiv:1002.0010 [hep-ph]; S. Jadach and M. Skrzypek, arXiv:0909.5588 [hep-ph], arXiv:0905.1399 [hep-ph].

[57] A.D. Martin, M.G. Ryskin and G. Watt, Eur. Phys. J. C **66** (2010) 163.

[58] C. Flensburg and G. Gustafson, arXiv:1004.5502 [hep-ph]; G. Gustafson, Acta Phys. Polon. B **40** (2009) 1981.

[59] F. Hautmann, Acta Phys. Polon. B **40** (2009) 2139.

[60] F. Hautmann and H. Jung, arXiv:0804.1746 [hep-ph], in Proc. 8th International Symposium on Radiative Corrections RADCOR2007 (Florence, October 2007).

[61] F. Hautmann, arXiv:0909.1240 [hep-ph].

[62] H. Jung et al., arXiv:1009.5067 [hep-ph].

[63] M. Deak et al., arXiv:1006.5401 [hep-ph]; F. Hautmann, Phys. Lett. B **535** (2002) 159; F. Hautmann, H. Jung and V. Pandis, arXiv:1011.6157 [hep-ph].

[64] ATLAS Collaboration, arXiv:1009.5908 [hep-ex].

[65] CMS Collaboration, arXiv:1010.0203 [hep-ex].

[66] M. Hentschinski, private communication.

[67] H.L. Lai et al. [CTEQ Collaboration], Eur. Phys. J. **C12** (2000) 375.

[68] M. Cacciari and G.P. Salam, Phys. Lett. B **641** (2006) 57; M. Cacciari, G.P. Salam and G. Soyez, http://fastjet.fr; G.P. Salam and G. Soyez, JHEP **0705** (2007) 086.

[69] S. Alioli et al., arXiv:1012.3380 [hep-ph].

[70] A. Papaefstathiou, J.M. Smillie and B.R. Webber, JHEP **1004** (2010) 084.

[71] I. Sung, Phys. Rev. D**80** (2009) 094020.

[72] Y. Hatta and T. Ueda, Phys. Rev. D**80** (2009) 074018.

[73] S. Catani, M. Ciafaloni and F. Hautmann, Phys. Lett. B**307** (1993) 147.

[74] T. Becher and M. Neubert, arXiv:1007.4005 [hep-ph]; S. Mantry and F. Petriello, arXiv:1011.0757 [hep-ph].

[75] P.J. Mulders and T.C. Rogers, Phys. Rev. D**81** (2010) 094006.

[76] A. Idilbi and I. Scimemi, arXiv:1009.2776 [hep-ph]; arXiv:1012.4419 [hep-ph].

[77] I. Cherednikov and N. Stefanis, Phys. Rev. D**80** (2009) 054008.

[78] A. Bacchetta, D. Boer, M. Diehl and P.J. Mulders, JHEP **0808** (2008) 023.

[79] T.C. Rogers, Phys. Rev. D**78** (2008) 074018.

[80] F. Hautmann, Phys. Lett. B**655** (2007) 26; arXiv:0708.1319; J.C. Collins and F. Hautmann, JHEP **0103** (2001) 016; Phys. Lett. B**472** (2000) 129.

[81] A. Aktas et al., Eur. Phys. J. C**46** (2006) 27; S. Chekanov et al., Phys. Lett. B**632** (2006) 13.

[82] A. Knutsson, LUNFD6-NFFL-7225-2007 (2007); L. Jönsson, AIP Conf. Proc. 828 (2006) 175.

[83] F.D. Aaron et al., Eur. Phys. J. C**54** (2008) 389.

Top-left panel: $\Delta\eta=2$, legend: CASCADE, PYTHIA-Perugia-hard, PYTHIA-noMPI. Axes: $d\sigma/dcos\Delta\phi$ vs $cos\Delta\phi$.

Top-right panel: $\Delta\eta=3$.

Bottom-left panel: $\Delta\eta=4$. LHC sqrt(s)=7000, jet $E_T>10$ GeV, central and fwd jets.

Bottom-right panel: $\Delta\eta=5$.

Top-left panel ($\Delta\eta=2$):
- $d\sigma/dcos\Delta\phi$ (y-axis)
- CASCADE
- PYTHIA-Perugia-hard
- PYTHIA-noMPI
- $\cos\Delta\phi$ (x-axis)

Top-right panel ($\Delta\eta=3$):
- $d\sigma/dcos\Delta\phi$ (y-axis)
- $\cos\Delta\phi$ (x-axis)

Bottom-left panel ($\Delta\eta=4$):
- $d\sigma/dcos\Delta\phi$ (y-axis)
- $\cos\Delta\phi$ (x-axis)

Bottom-right panel ($\Delta\eta=5$):
- $d\sigma/dcos\Delta\phi$ (y-axis)
- LHC sqrt(s)=7000
- jet E_T>30 GeV
- central and fwd jets
- $\cos\Delta\phi$ (x-axis)